NEUROSCIENCE
RESEARCH ARTICLE
J. I. Szu et al. / Neuroscience 428 (2020) 140–153

Aquaporin-4 Dysregulation in a Controlled Cortical Impact Injury Model of Posttraumatic Epilepsy

Jenny I. Szu, Som Chaturvedi, Dillon D. Patel and Devin K. Binder*

Center for Glial-Neuronal Interactions, Division of Biomedical Sciences, School of Medicine, University of California, Riverside, CA, USA

Abstract—Posttraumatic epilepsy (PTE) is a long-term negative consequence of traumatic brain injury (TBI) in which recurrent spontaneous seizures occur after the initial head injury. PTE develops over an undefined period during which circuitry reorganization in the brain causes permanent hyperexcitability. The pathophysiology by which trauma leads to spontaneous seizures is unknown and clinically relevant models of PTE are key to understanding the molecular and cellular mechanisms underlying the development of PTE. In the present study, we used the controlled-cortical impact (CCI) injury model of TBI to induce PTE in mice and to characterize changes in aquaporin-4 (AQP4) expression. A moderate-severe TBI was induced in the right frontal cortex and video-electroencephalographic (vEEG) recordings were performed in the ipsilateral hippocampus to monitor for spontaneous seizures at 14, 30, 60, and 90 days post injury (dpi). The percentage of mice that developed PTE were 13%, 20%, 27%, and 14% at 14, 30, 60, and 90 dpi, respectively. We found a significant increase in AQP4 in the ipsilateral frontal cortex and hippocampus of mice that developed PTE compared to those that did not develop PTE. Interestingly, AQP4 was found to be mislocalized away from the perivascular endfeet and towards the neuropil in mice that developed PTE. Here, we report for the first time, AQP4 dysregulation in a model of PTE which may carry significant implications for epileptogenesis after TBI.

Key words: posttraumatic epilepsy, spontaneous seizure, traumatic brain injury, controlled cortical impact injury, aquaporin-4, Kir4.1.

INTRODUCTION

Posttraumatic epilepsy (PTE) is a long-term negative consequence of traumatic brain injury (TBI) in which recurrent spontaneous seizures occur after the initial head injury (Pitkänen and McIntosh, 2006). PTE accounts for approximately 20% of symptomatic epilepsy (Engel, 2001; Lowenstein, 2009) and 6% of all epilepsies (Hauser et al., 1993). Epidemiologic studies show that PTE develops in 30% of individuals between the ages of 15 and 35, 14% of children under the age of 14, and 8% of adults over the age of 65 (Hauser et al., 1993). It is also widely agreed that severity of injury is strongly correlated with an increased risk of developing PTE (Jennett and Lewin, 1960; Annegers et al., 1998). Examples of severe head injuries that have a clear association with late seizure development include penetrating head injuries, brain contusions, and/or subdural hematomas (Temkin, 2003). In fact, the prevalence of PTE is ~50% in 20th century war veterans due to their increased exposure to penetrating head injuries (Salazar et al., 1985; Raymont et al., 2010). Unfortunately, the pathophysiology by which trauma leads to spontaneous seizures is unknown and clinically relevant models of PTE are key to understanding the molecular and cellular mechanisms underlying the development of PTE.

From a modeling perspective, the pathophysiology and heterogeneity of TBI and epilepsy creates a tremendous challenge for researchers. In addition to injury severity, other factors that may contribute to the overall effect of TBI include, but are not limited to, age, sex, pre-existing conditions, and genetics (Pitkänen and McIntosh, 2006). Although experimental models of PTE cannot entirely represent the human condition, they are valuable in studying the cellular and molecular aspects of PTE. Moreover, animal models can be utilized to develop and characterize new therapeutic strategies. In fact, the development of spontaneous seizures and PTE have been reported in experimental models using the three widely used models of TBI: fluid percussion injury

*Corresponding author. Address: Division of Biomedical Sciences, School of Medicine, University of California, 1247 Webber Hall, Riverside, CA 92521, USA.
E-mail address: dbinder@ucr.edu (D. K. Binder).

Abbreviations: AQP4, aquaporin-4; BBB, blood–brain barrier; CNS, central nervous system; CSF, cerebrospinal fluid; CCI, controlled cortical impact; dpi, days post injury; EPSC, excitatory postsynaptic current; ECS, extracellular space; FPI, fluid percussion injury; GFAP, glial fibrillary acid protein; IHC, immunohistochemistry; i.p., intraperitoneal; kDa, kiloDalton; MFS, mossy fiber sprouting; PTE, posttraumatic epilepsy; SE, status epilepticus; TLE, temporal lobe epilepsy; T-lectin, tomato-lectin; TBI, traumatic brain injury; vEEG, video-electroencephalographic; WT, wild-type.

https://doi.org/10.1016/j.neuroscience.2019.12.006
0306-4522/

(FPI) (D'Ambrosio et al., 2004; Kharatishvili et al., 2006; Curia et al., 2010; Bolkvadze and Pitkänen, 2012), weight-drop injury (Nilsson et al., 1994; Golarai et al., 2001; Shandra et al., 2019), and controlled cortical impact (CCI) injury (Hunt et al., 2009, 2010; Bolkvadze and Pitkänen, 2012; Guo et al., 2013). Although research efforts have attempted to determine potential mechanisms underlying PTE, limited studies have identified the cellular or molecular underpinnings of epileptogenesis after TBI.

It is now well documented that changes in astrocytes may play a critical role in the development of epilepsy. Two key players are the astrocytic water channel aquaporin-4 (AQP4) and the inwardly rectifying K^+ channel Kir4.1. AQP4 is primarily expressed in both brain and spinal cord astrocytes (Manley et al., 2004; Verkman et al., 2006) and facilitates the bidirectional transport of water in response to an osmotic gradient (Tait et al., 2008). AQP4 is found highly polarized to astrocytic endfeet in contact with blood vessels (Verkman et al., 2006; Nagelhus and Ottersen 2013) and is involved in water movement between blood and brain and brain and cerebrospinal fluid (CSF) compartments (Manley et al., 2004). In astrocytes, Kir4.1 maintains K^+ homeostasis by either net uptake or spatial buffering (MacAulay and Zeuthen, 2012; Steinhäuser et al., 2012; Cheung et al., 2015). In the K^+ spatial buffering model, locally released K^+ ions following neuronal activity are taken up by astrocytes, redistributed across the astroglial syncytium via gap junctions, and transferred to areas of low K^+ concentration (Orkand, 1986; Kofuji and Newman 2004).

Previous reports have suggested a direct interaction between AQP4 and Kir4.1 primarily in the perivascular membranes where the endfeet of astrocytes are in contact with blood vessels (Nagelhus et al., 1999, 2004, Connors and Kofuji, 2006; Ruiz-Ederra et al., 2007; Masaki et al., 2010). Based on their cellular and subcellular localization, functional coupling between water transport and potassium clearance has been hypothesized in central nervous system (CNS) disorders. For example, impaired astrocyte-dependent water homeostasis has been implicated in epilepsy. In brief, during neuronal activity, extracellular potassium is taken up by Kir4.1 accompanied by water entry through AQP4 to maintain osmotic balance. K^+ is then redistributed via potassium spatial buffering and water is released into the perivascular space through AQP4 expressed at astrocytic endfeet. In an epileptic brain, perivascular AQP4 is mislocalized towards the neuropil, thus resulting in astrocytic swelling, decreased extracellular space (ECS), and increased ephaptic interactions (Wetherington et al., 2008; Binder et al., 2012). Indeed, patients with mesial temporal lobe epilepsy (TLE) displayed loss of perivascular AQP4 (Eid et al., 2005) and Kir4.1 (Heuser et al., 2012).

In the present study, we used the well-established CCI model of PTE to monitor for spontaneous seizures and subsequently, the development of PTE in mice at 14, 30, 60, and 90 days post injury (dpi). Using chronic *in vivo* video-electroencephalographic (vEEG) recordings, we quantified the number of spontaneous seizures and PTE. Additionally, AQP4 and Kir4.1 regulation was also investigated at each time point using Western blot analysis and immunohistochemistry (IHC).

EXPERIMENTAL PROCEDURES

Animals

All experiments were conducted in accordance with National Institutes of Health guidelines and approved by the University of California, Riverside Institutional Animal Care and Use Committee. Adult male CD1 wild-type (WT) between the ages of 8–10 weeks old were used for all experiments. The mice were housed under a 12-h light/dark cycle with water and food provided *ad libitum*. A total of 95 mice were used for this study (n = 47 TBI and n = 48 sham).

Study design

Experimental endpoints of 14, 30, 60, and 90 dpi were chosen to better understand the temporal progression of PTE. A separate cohort of mice was used for each time point. At day 0, mice were subjected to a single CCI. Sham mice received a craniotomy only. 10 days prior to each experimental endpoint, mice received an electrode implanted in their ipsilateral dorsal hippocampus. After 3 days of recovery, mice underwent vEEG recordings for 1 week. At each experimental endpoint, mice were sacrificed for Western blot analysis or IHC. The study design is summarized in Fig. 1.

CCI injury

Mice were anesthetized with an intraperitoneal (i.p.) injection of ketamine and xylazine (80 mg/kg ketamine, 10 mg/kg xylazine). Additional anesthesia was administered only when necessary. Once an adequate plane of anesthesia was achieved, the hairs on the scalp was removed using clippers and depilatory cream. The scalp was then disinfected with betadine solution and cleaned with 70% ethanol. Mice were then mounted onto a stereotactic frame and a midline incision was made and reflected. The fascia was gently removed and the skull was cleaned with normal saline.

With a high-speed surgical hand drill and a ¼ mm HP-sized carbide bur (SS White) a craniotomy of $\sim 2 \times 2$ mm^2 was created over the right frontal cortex with the dura intact. A moderate-severe TBI was then induced with a CCI device (Leica Biosystems) onto the exposed brain with a 2 mm flat impactor tip at a velocity of 5 m/s, a depth of 1 mm, and a contact time of 200 ms. After the injury, the skull flap was carefully replaced and the incision was sutured. Mice were then allowed to recover over a temperature-controlled heating pad.

Electrode preparation

A 3-channel two twisted stainless steel electrode (Plastics One) was used for all EEG surgeries and prepared as previously described (Lapato et al., 2017). The twisted bipolar wires were cut to 2 mm for implanting into the dor-

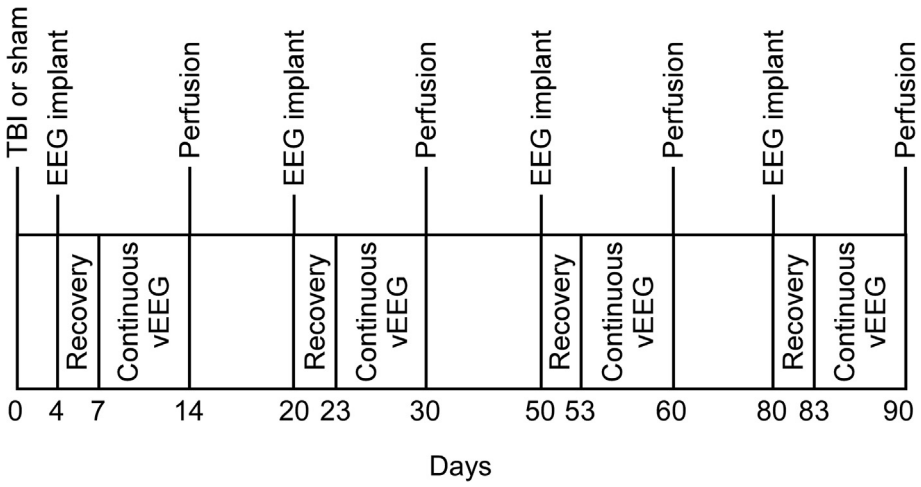

Fig. 1. Summary of study design. In brief, mice were subjected to a TBI or craniotomy (for sham groups) at day 0. 10 days before each experimental endpoint (14, 30, 60 and 90 days), mice were implanted with an indwelling hippocampal electrode. After 3 days of recovery, mice underwent continuous vEEG recordings. At each final time point, the mice were perfused for IHC or Western blot analysis. A separate cohort of mice was used for each time point.

sal hippocampus and the untwisted wire was cut to ~0.5 mm to ground in the cortex. To ensure high-fidelity EEG recordings, ~0.5 mm of the insulating coat was removed at the distal tip of all wires. The electrodes were then sterilized with 70% ethanol and the ground position on top of the implant pedestal was marked to ensure proper placement of the pins during EEG acquisition.

Electrode implantation

Mice underwent EEG implant surgery 10 days prior to their final time point (14, 30, 60, and 90 dpi). Mice were anesthetized as described above and immobilized in a stereotactic frame. The sutures were removed and the scalp was reflected. The skull was then cleaned with normal saline. To create a greater surface area for cementing the electrode, etching gel was applied to the skull for ~10 s and washed 2–3 times with normal saline. Using a high-speed surgical hand drill with a ¼ mm HP-sized carbide bur (SS White) a craniotomy of ~2 mm in diameter (to accommodate the distance between the recording and ground wires) was created between over the right frontal bone. The skull flap was gently removed without damage to the underlying dura and the bone dust was washed off with normal saline. The dura was then carefully detached using a 27 G needle and bonding agent (Clearfil Photobond) was applied onto the skull with a microbrush (without contact to the exposed brain) and light cured for 20 s. The electrode was then slowly lowered into the hippocampus (AP = −1.8 mm, ML = +1.6 mm from bregma) until the implant pedestal rested gently on top of the skull. To secure the electrode in place, dental cement (Panavia SA cement) was applied across the skull surface and surrounding the implant and light cured for 20 seconds, followed by additional cement as necessary. After completion of electrode implantation, the animals recovered for 3 days.

Continuous vEEG acquisition

vEEG acquisition began 3 days after electrode implantation and lasted 7 days. In the sham group, the total number of mice that underwent vEEG is 7, 6, 12, and 7 for 14, 30, 60, and 90 days post craniotomy, respectively. In the TBI group, the total number of mice that underwent vEEG is 8, 10, 11, and 7 for 14, 30, 60, and 90 dpi, respectively. During vEEG recording, mice were single housed with access to food and water *ad libitum* and freely moving. Behavioral activity was video monitored with a megapixel IP camera (HD 1080P) with infrared LED for night time recording (ELP1 CCTV) and time synced with EEG recording. Mice were recorded using either our customized wireless EEG sensor (BioPac) or a tethered system (BioPac). For wireless EEG recordings, a wireless transmitter (Epoch) was attached to the implanted EEG pedestal and the cage was placed on top of a receiving tray. For tethered EEG recordings, mice were connected to the acquisition system via commutator to allow for freedom of motion. Both wireless and tethered EEG recordings were obtained using a digital acquisition system (MP150 or MP160, Acqknowledge 4.4 or Acqknowledge 5 software). Normal EEG output was amplified with a gain of 5000, bandpass filtered from 0.1 to 35 Hz, and digitized at 625 samples/s.

Confirmation of spontaneous seizures and PTE

Electrographic spontaneous seizures from the 1-week vEEG recordings were manually identified and confirmed by two blinded observers. Spontaneous seizures were defined as spiking epileptiform activity lasting continuously for at least 5 seconds at a frequency of ≥3 Hz (Lee et al., 2012). Electrographic seizures were also correlated with corresponding time-synced video for behavioral assessment based on the modified Racine scale (Table 1) (Ihara et al., 2016). Post-traumatic seizures are characterized based on the time they occurred after the initial TBI: immediate posttraumatic seizures, within 24 h post injury; early posttraumatic

Table 1. Modified Racine scale for classification of behavioral seizures

Score	Behavioral stage
0	No behavioral change
1	Sudden behavioral arrest with orofacial automatism
2	Head nodding
3	Forelimb clonus with lordotic posture
4	Forelimb clonus with rearing and falling
5	Generalized tonic-clonic activity with loss of postural tone

seizures, between 24 h and 1 week post injury; and late posttraumatic seizures, at least 1 week post injury and represents the true manifestation of PTE. Mice with two or more late spontaneous seizures during the 1-week vEEG were classified as having PTE.

Seizure frequency, duration, and incidence of PTE

Seizure frequency was determined for all mice that developed spontaneous seizures and was calculated as the ratio of the total number of seizures/7 (total number of vEEG recording days) for each mouse. The mean seizure frequency was analyzed with one-way ANOVA with Bonferroni's *post hoc* analysis. The mean seizure duration was analyzed with Kruskal–Wallis test. The total number (sum) of mice that developed spontaneous seizures, seizures, and total number of mice that developed PTE were also determined. All error bars are represented as mean ± standard error of the mean (SEM) and differences were considered statistically significant when p value < 0.05.

Western blot analysis

A subset of mice from both sham and TBI groups at each time point were used for Western blot analysis. Western blot analysis of the ipsilateral frontal cortex and hippocampus was performed on sham (n = 5–8) and injured mice (n = 5–11) for all time points. Mice were euthanized with Fatal Plus (Henry Schein), transcardially perfused with ice-cold PBS (pH 7.4) containing complete protease inhibitors (Thermo Fisher), and the ipsilateral and contralateral frontal cortex and hippocampus were rapidly dissected. Harvested tissue was then homogenized with the Bullet Blender (Next Advance) in radioimmunoprecipitation assay (RIPA) buffer (Sigma) with complete protease inhibitors (Thermo Fisher) and centrifuged at 10,000 RPM for 10 min at 4 °C. Protein concentrations were assayed using the Micro BCA Protein Assay Kit (Thermo Fisher). Twenty micrograms of total protein was loaded and resolved by SDS–PAGE with 10% polyacrylamide and transferred to a 0.45 μm nitrocellulose membrane (Biorad). Membranes were then dried between two filter papers for 30 min, blocked in 5% milk in TBST for 1 h, and incubated in primary antibodies overnight in 4 °C for AQP4 (1:1000, Millipore AB3594), Kir4.1 (1:400, Alomone APC-035), and β-actin (1:10,000, Sigma A1978) which served as an internal control. Finally, membranes were incubated in species-specific secondary IR Dye for 1 h and imaged using the Li-COR Odyssey Fc Western Imaging System.

Bands were visualized and quantified using the Li-COR Odyssey Fc Western Imaging System and protein levels were normalized to β-actin levels. For AQP4 and Kir4.1, the monomer bands ~30 kDa and ~42 kDa, respectively, are shown and quantified with GraphPad Prism 8. Comparisons between sham and TBI groups were analyzed with two-way ANOVA with Bonferroni *post hoc* analysis. All error bars are represented as mean ± SEM and differences were considered statistically significant when p value < 0.05.

Immunohistochemistry

A subset of mice from both sham and TBI groups at each time points were used for IHC. Tissue processing and imaging were performed blinded for all groups and time points (n = 4–5, sham and n = 4, TBI). Mice were euthanized with Fatal Plus (Henry Schein) and transcardially perfused with ice-cold PBS (pH, 7.4) followed by 4% paraformaldehyde (PFA; pH 7.4). Brains were rapidly dissected, postfixed in 4% PFA overnight at 4 °C followed by cryoprotection in 30% sucrose in PBS at 4 °C. Brains were then frozen with ice-cold isopentane and stored in −80 °C until they were cut to 50 μm coronal sections using a cryostat (Leica CM 1950, Leica Microsystems). Sections were stored in 0.02% sodium azide in PBS at 4 °C and all slices were processed simultaneously. Alternating sections away from the electrode track mark were chosen for staining. Sections were washed with PBS, blocked with 5% normal goat serum in 0.1 M PBS for 1 h and incubated with tomato-lectin (T-lectin, 1:200), primary antibody for AQP4 (1:200, Millipore AB2218), and glial fibrillary acidic protein (GFAP, 1:200, Millipore MAB360) in 0.3% Triton X-100 for 2 days at 4 °C. After washing with PBS, sections were incubated with species-specific secondary antibody conjugated with Alexa 594 and Alexa 647 (Life Technologies) for visualization and then mounted with in ProLong Antifade kit without DAPI (Invitrogen). 63× images of the ipsilateral frontal cortex and the hippocampus (stratum radiatum and stratum lacunosum moleculare) were obtained using a confocal microscope (Leica TCS SP5). Confocal images of the frontal cortex were taken in the perilesional cortex where cortical tissue was preserved from the injury.

RESULTS

Injury severity after TBI

This CCI model of TBI induces a moderate-severe injury. A total of 53 mice received a TBI with a mortality of 11%. The low mortality rate is one of the advantages of using CCI as a model of TBI (Dixon et al., 1991). In some mice, the dura was ruptured which resulted in substantial bleeding and immediate brain swelling, indicative of vasogenic edema. In cases where the dura was not ruptured, subdural hematoma and hemorrhage were evident. One histopathological hallmark of TBI is the appearance of astrogliosis. We observed upregulation of GFAP immunoreactivity at the injury site at all time points after injury as well as some tissue deformation from the impact (Fig. 2).

Spontaneous seizures after TBI

To establish a working model of PTE, spontaneous recurrent seizures must be observed at least 1 week after the initial trauma. Electrographic spontaneous seizures were detected at each time point after TBI and correlated with corresponding video for behavioral assessment. Nonconvulsive seizures were observed that correlated with the electrographic seizures (Videos 1 and 2). Behaviorally, seizures were characterized

primarily by motor arrest with occasional facial clonus based on the modified Racine scale (Table 1) (Ihara et al., 2016). Sham mice remained seizure-free with the exception of one mouse which displayed a single spontaneous seizure at 60 days post craniotomy. No sham mice exhibited PTE.

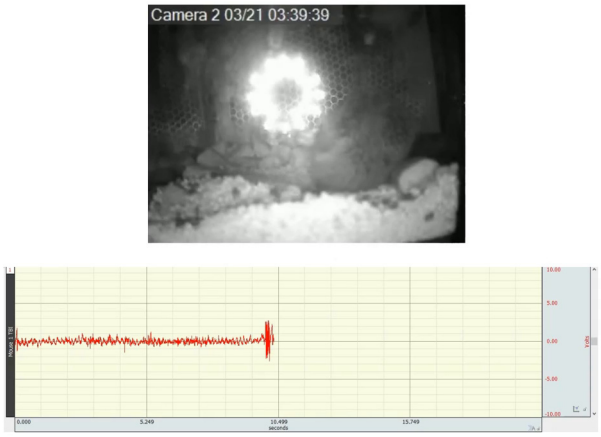

Video 1. Electrographic spontaneous seizure at 30 dpi. vEEG of a mouse with spontaneous seizure 30 dpi. Baseline EEG was correlated with normal behavior which was interrupted by a sudden spontaneous electrographic seizure (starting at ~10 s on the time scale) that was associated with motor arrest. Baseline EEG returned at the end of the seizure with resumption of normal behavior. The seizure duration was ~7 s. dpi = days post injury.

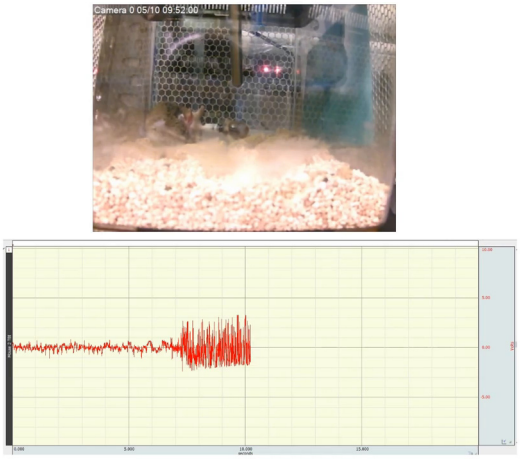

Video 2. Electrographic spontaneous seizure at 60 dpi. vEEG of a mouse with spontaneous seizure 60 dpi. Baseline EEG was associated with movement of the animal with sudden behavioral arrest that was associated with a spontaneous electrographic seizure (starting at ~7 s on the time scale). Normal behavior resumed at the end of the electrographic seizure. The seizure duration was ~6 s. dpi = days post injury.

Electrographically, most seizure onset was sudden with increased EEG frequency and amplitude (fast polyspike) followed by return to baseline. Other seizures observed either initiated from a ramp-up of baseline and developed into a full seizure or displayed spikes of at least 3 Hz. Fig. 3 shows different electrographic seizure morphologies captured during the 1-week vEEG recording.

The mean seizure frequency per day at 14, 30, 60 and 90 dpi are 0.5714 ± 0.000, 0.3810 ± 0.1717, 0.7143 ± 0.2333, and 0.4286 ± 0.2857, respectively ($F(3,6) = 0.4493$, $p = 0.7270$). The mean seizure duration at 14, 30, 60 and 90 dpi are 23.25 ± 8.076 s, 19.00 ± 5.704 s, 12.50 ± 1.647 s, and 9.667 ± 1.909 s, respectively ($p = 0.2725$). The number of mice that developed spontaneous seizures are 1/8 (13%), 3/10 (30%), 4/11 (36%), and 2/7 (29%) at 14, 30, 60, and 90 dpi, respectively. The total number of seizures are 4, 8, 20, and 6 at 14, 30, 60, and 90 dpi respectively (Table 2).

It is expected that not all TBI will result in the development of PTE. Thus, the total number of mice that developed PTE (having 2 or more spontaneous seizures during the 1-week vEEG recording) was also determined. The total number of mice that developed PTE are 1/8 (13%), 2/10 (20%), 3/11 (27%), and 1/7 (14%) at 14, 30, 60, and 90 dpi, respectively (Table 2).

Increased AQP4 in the frontal cortex and hippocampus of mice with PTE

No significant differences in Kir4.1 (Fig. 4) and AQP4 (Fig. 5) expression levels were detected in the frontal cortex and hippocampus between sham and TBI groups at all time points. Kir4.1 expression levels were not statistically different in both the frontal cortex and hippocampus between mice with and without PTE (Fig. 6A). Interestingly, however, a significant increase in AQP4 expression was detected in both the frontal cortex and hippocampus of mice that developed PTE compared with mice that did not develop PTE (Fig. 6B). Contralateral AQP4 and Kir4.1 expression was also analyzed but no statistical differences were observed between sham and TBI at all time points (data not shown). Additionally, because EEG recordings were only performed in the ipsilateral hippocampus, changes in AQP4 and Kir4.1 expression in the contralateral hippocampus were not investigated in mice with and without PTE.

Mislocalization of AQP4 in mice with PTE

To further investigate the increased AQP4 expression in mice with PTE, 63X confocal images were obtained. As expected, colocalization of AQP4 with blood vessels were abundant in the frontal cortex and hippocampus (Fig. 7) of sham mice. In the frontal cortex, marked loss of perivascular AQP4 was evident at 14 and 90 dpi in mice that did not develop PTE, however, a partial recovery of perivascular AQP4 was detected 30 and 60 dpi (Fig. 8 *top*). On the other hand, mislocalization of AQP4 was detected in the frontal cortex of mice that did develop PTE at 14 dpi with only partial redistribution of AQP4 at 30 and 60 dpi (Fig. 8 *bottom*). In the hippocampus of mice without PTE, perivascular AQP4

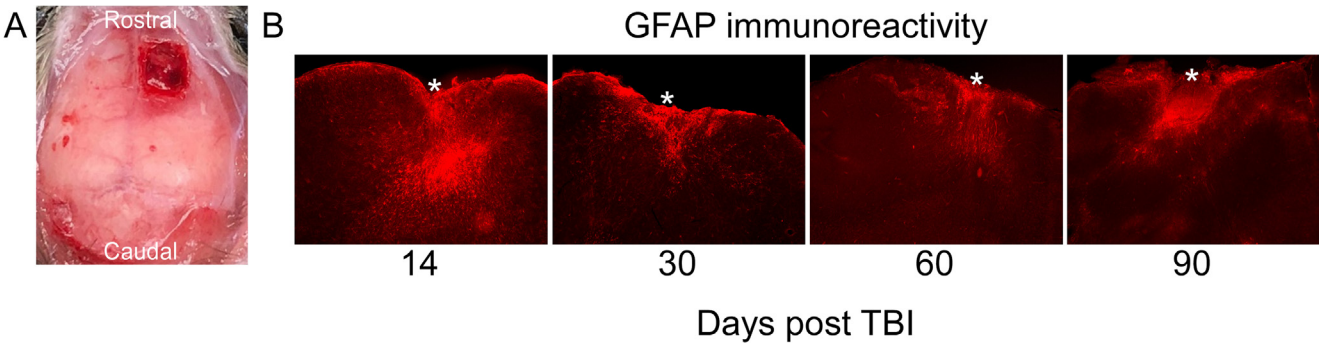

Fig. 2. Injury severity after CCI. (**A**) In this example, the dura is intact and subdural hematoma and hemorrhage can be seen immediately after TBI. In other cases, dura rupture, severe bleeding, and immediate brain swelling indicative of vasogenic edema can be seen (data not shown). (**B**) Coronal view of the ipsilateral frontal cortex after TBI. Increased GFAP immunoreactivity indicative of reactive astrocytes, is observed after TBI at all time points. Tissue deformation (represented by asterisks denoting site of injury) can also be observed on the cortical surface. Images taken at 5×.

was mostly preserved with only a few blood vessels lacking AQP4 (Fig. 9 *top*). In contrast, in mice with PTE, hippocampal AQP4 dysregulation was observed primarily at 14 dpi where AQP4 immunoreactivity was largely expressed in the soma and major processes of astrocytes and blood vessels were denuded of perivascular AQP4 expression (Fig. 9 *bottom*). At 30 dpi, an intermediate recovery of perivascular AQP4 expression was observed in mice with PTE, whereas at 60 dpi, perivascular AQP4 was indistinguishable from the mice without PTE (Fig. 9 *bottom*). Because only a single mouse developed PTE at 14 and 90 dpi, the tissue was used for IHC and Western blot, respectively.

DISCUSSION

In the present study, we used the CCI injury model of PTE in which a single moderate-severe TBI induced in the right frontal cortex led to spontaneous recurrent seizures in the ipsilateral hippocampus, a region distant from the injury location. Mice underwent 1-week of vEEG recordings and key epileptogenic astrocytic channels AQP4 and Kir4.1 was investigated using Western blot analysis and IHC. The main findings from these studies are the following: (1) successful implementation of CCI-based PTE in mice with chronic vEEG generated, for the first time, 13%, 20%, 27%, and 14% of mice with PTE at 14, 30, 60, and 90 dpi, respectively (the highest yield of PTE yet reported with chronic vEEG analysis); and (2) significant upregulation and mislocalization of AQP4 in the frontal cortex and hippocampus of mice with PTE compared to mice without PTE, suggesting possible contribution of AQP4 dysregulation to epileptogenesis after TBI.

Spontaneous seizures after CCI

The frontal lobe was chosen as the location for the TBI due to its impact on epileptogenesis. Human and preclinical studies have shown frontal lesions as a significant risk factor for PTE (Pohlmann-Eden and Bruckmeir, 1997; Hudak et al., 2004; D'Ambrosio et al., 2005; Curia et al., 2010). In humans, the probability of late posttraumatic seizures from a unilateral contusion in the frontal, temporal, and parietal locations are 20%, 16%, and 19%, respectively; whereas in bilateral contusions, the risk for epilepsy from frontal, temporal, and parietal locations are 26%, 31%, and 66%, respectively (Englander et al., 2003). Additionally, studies in rats found that compared with injury induced in the medial-parietal and caudal-parietal cortex, TBI in the rostral-parietal cortex resulted in higher seizure frequency (Curia et al., 2010). Based on these findings, it is expected that mice in these studies would yield a higher probability of developing epilepsy from a brain injury arising in the frontal cortex.

The CCI model has shown promise as a model of PTE after TBI. Studies utilizing this model have reported spontaneous seizures after injury however it is important to note that in these studies the injury was induced over the parietotemporal region where the underlying hippocampus is most susceptible to injury, even with different impact depths. Indeed, significant alterations in hippocampal morphology after TBI were reported with overt mossy fiber sprouting (Hunt et al., 2009, 2010; Bolkvadze and Pitkänen, 2012) Most notably, in our studies, the hippocampus did not undergo drastic morphological changes (data not shown), yet we were able to detect spontaneous seizures in the hippocampus after a single TBI in the frontal cortex. Therefore, in our study, it is plausible that the injury in the frontal cortex led to the development of spontaneous hippocampal seizures which may be caused by local recurrent excitatory connections, particularly at the later time points (30 and 60 dpi) when increased incidence of spontaneous seizures was observed.

Experimental studies have also found that the frontal cortex is particularly vulnerable to seizures regardless of injury location. After FPI in the rostral-parietal cortex, the incidence and severity of seizures arising from the frontal cortex were higher compared to seizures in the parietal or occipital cortices. Furthermore, limbic seizures were found to proceed more slowly (several months after TBI) than cortical seizures (D'Ambrosio et al., 2005; Curia et al., 2010). In our studies, a single electrode was used to monitor for hippocampal seizures after TBI in the frontal cortex. Although spontaneous sei-

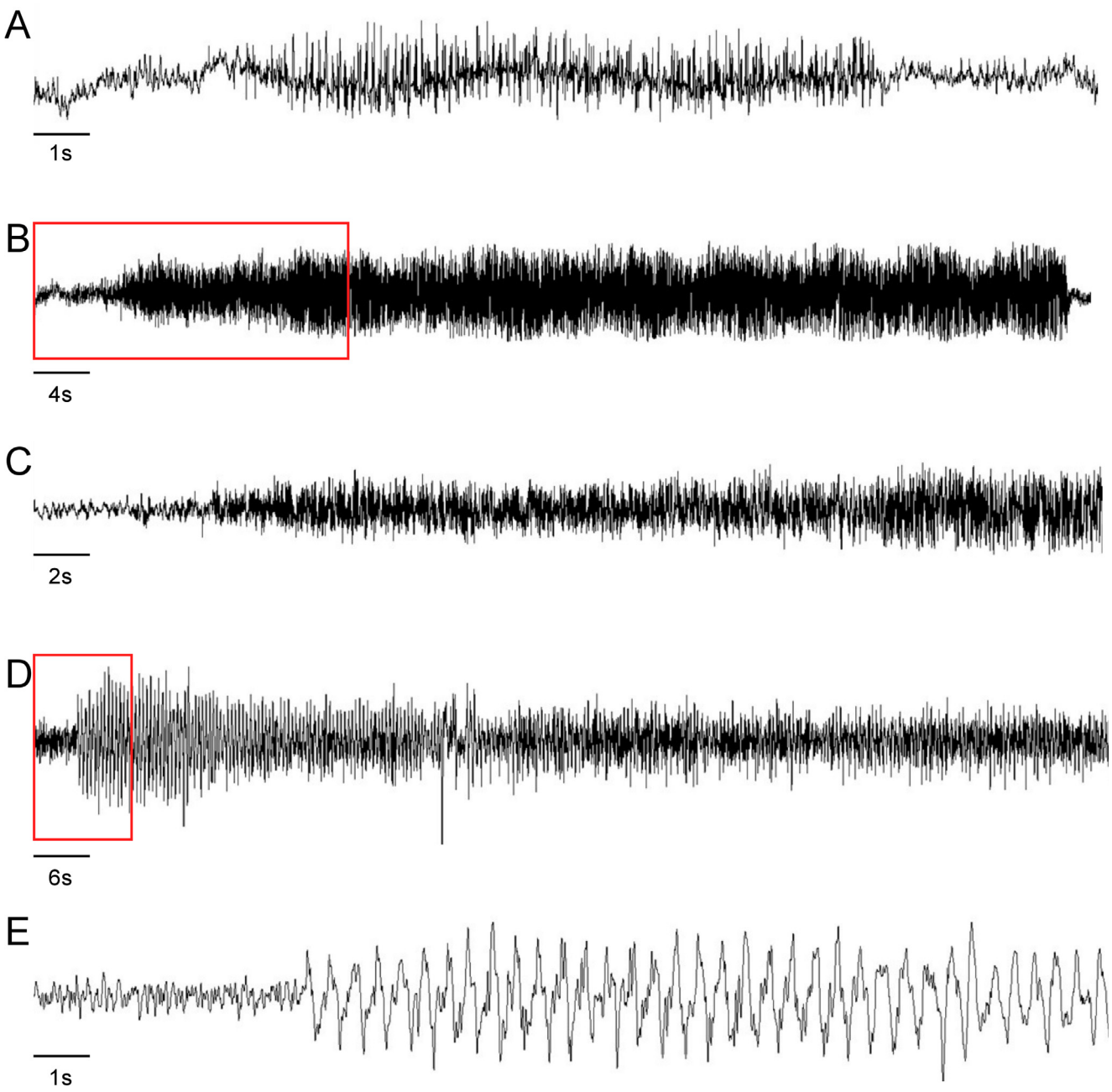

Fig. 3. Morphology of electrographic spontaneous seizures. Examples of different electrographic seizure morphologies. (**A**) Typical spontaneous seizure with increased frequency and amplitude (fast polyspike) followed by return to baseline. (**B**) A seizure initiated from a ramp-up of baseline and developed into full seizure. (**C**) Expanded EEG from red boxed area in (**B**) demonstrating baseline gradually increasing in amplitude and progressing into a full seizure. (**D**) A seizure exhibiting 3 Hz spikes. (**E**) Expanded EEG from red boxed area in (**D**).

Table 2. Seizure frequency, duration, and incidence of PTE. The total number (sum) of mice that developed spontaneous seizures, number of seizures, and mice with PTE were determined. The seizure frequency and duration are represented as mean ± SEM

Timepoint	Number of mice with seizures	Number of seizures	Number of mice with PTE
14	1/8 (13%)	4	1/8 (13%)
30	3/10 (30%)	8	2/10 (20%)
60	4/11 (36%)	20	3/11 (27%)
90	2/7 (29%)	6	1/7 (14%)
Total	10/36 (36%)	38	7/36 (19%)

zures were observed as early as 14 dpi, the majority of the seizures were recorded at 60 dpi. One explanation for this may be the fact that the hippocampus is distant from the injury site (frontal cortex) and the injury sustained in the hippocampus is mild. Thus, seizures generating from the hippocampus may not be evident until later. Another possibility is that focal seizures that begin in the frontal neocortex can spread and kindle the hippocampus (D'Ambrosio et al., 2005; Curia et al., 2010) via cortico–cortico or cortico–subcortical pathways (D'Ambrosio et al., 2005). Thus, in our model, seizures may possibly

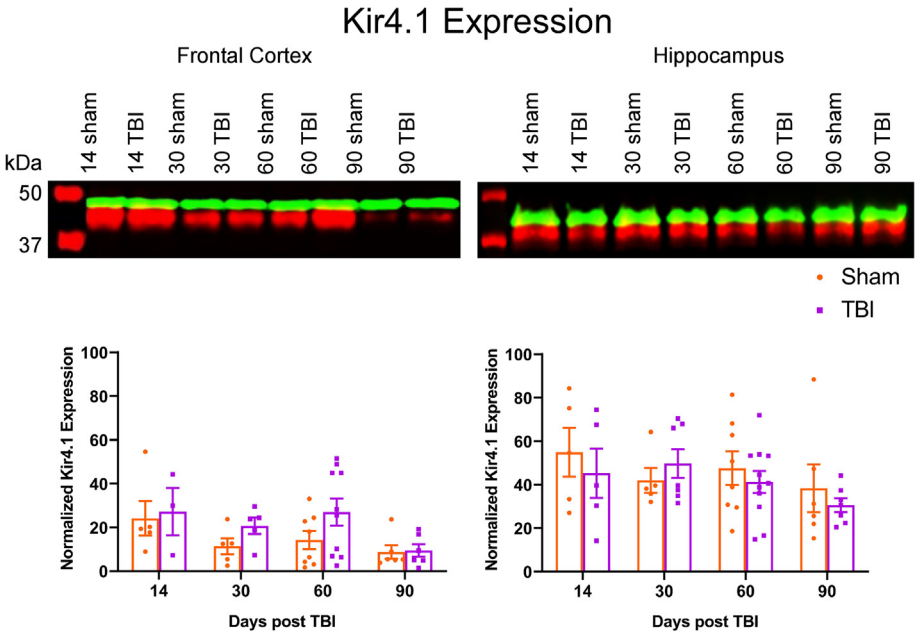

Fig. 4. TBI does not alter Kir4.1 protein levels in the frontal cortex and hippocampus. Overall Kir4.1 expression levels were not statistically different between sham and TBI groups at all time points. The monomer of Kir4.1 (~42 kDa, red band) is shown. β-Actin (~42 kDa, green band) served as internal control. dpi = days post injury, kDa = kiloDalton. (For interpretation of the references to color in this figure legend, the reader is referred to the web version of this article.)

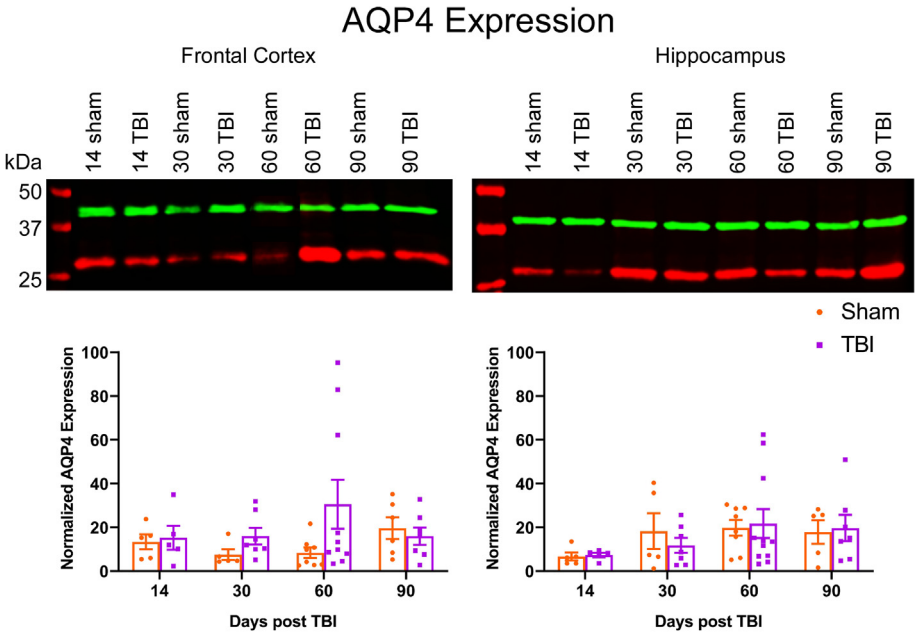

Fig. 5. TBI does not alter AQP4 protein levels in the frontal cortex and hippocampus. Overall AQP4 expression levels were not statistically different between sham and TBI groups at all time points. The monomer of AQP4 (~32 kDa, red band) is shown. β-Actin (~42 kDa, green band) served as internal control. dpi = days post injury, kDa = kiloDalton. (For interpretation of the references to color in this figure legend, the reader is referred to the web version of this article.)

initiate from the perilesional cortex (adjacent to the impact site) and spread to subcortical areas that would ultimately kindle connections to the hippocampus, making the hippocampus more susceptible to seizures at later times after the injury.

Contribution of perivascular AQP4 to spontaneous seizures and PTE

Although PTE remains a serious neuropathological sequela of TBI, the mechanisms by which spontaneous recurrent seizures occur following a brain injury remain unclear. Impaired water homeostasis is a defining characteristic in both TBI and epilepsy (D'Ambrosio et al., 1999; Guo et al., 2006; Binder et al., 2012; Devinsky et al., 2013). After a severe head injury, delayed onset of cerebral edema may develop which can increase intracranial pressure leading to deleterious consequences such as herniation and death (Maas et al., 2008; Donkin and Vink 2010). Additionally, the initial impact can cause vascular damage which can break down the blood–brain barrier (BBB), impair metabolic dysfunction, and alter ionic concentrations (Werner and Engelhard 2007; Chodobski et al., 2011) which may ultimately modulate neuronal excitability. Therefore, in this study, we asked whether a single TBI in the frontal cortex can lead to alterations in the key astrocytic proteins AQP4 and Kir4.1 which are known to regulate seizure activity in the hippocampus (Binder et al., 2012).

Due to their critical functions in water and K^+ homeostasis in the brain, AQP4 and Kir4.1 were investigated in our model of PTE. Western blot analysis revealed no significant differences in global AQP4 and Kir4.1 protein levels after TBI in both the frontal cortex and hippocampus. Because PTE was only detected in a subset of mice, we then asked whether differences in AQP4 and Kir4.1 exist between mice that developed PTE compared with mice that did not. No differences in Kir4.1 expression levels were detected in the frontal cortex and hippocampus of mice with and without PTE. Interestingly, AQP4 expression levels were significantly higher in both the frontal cortex and hippocampus of mice with PTE compared to mice that did not develop PTE. These findings suggest that AQP4 and Kir4.1 are distinctly regulated and that upregulation

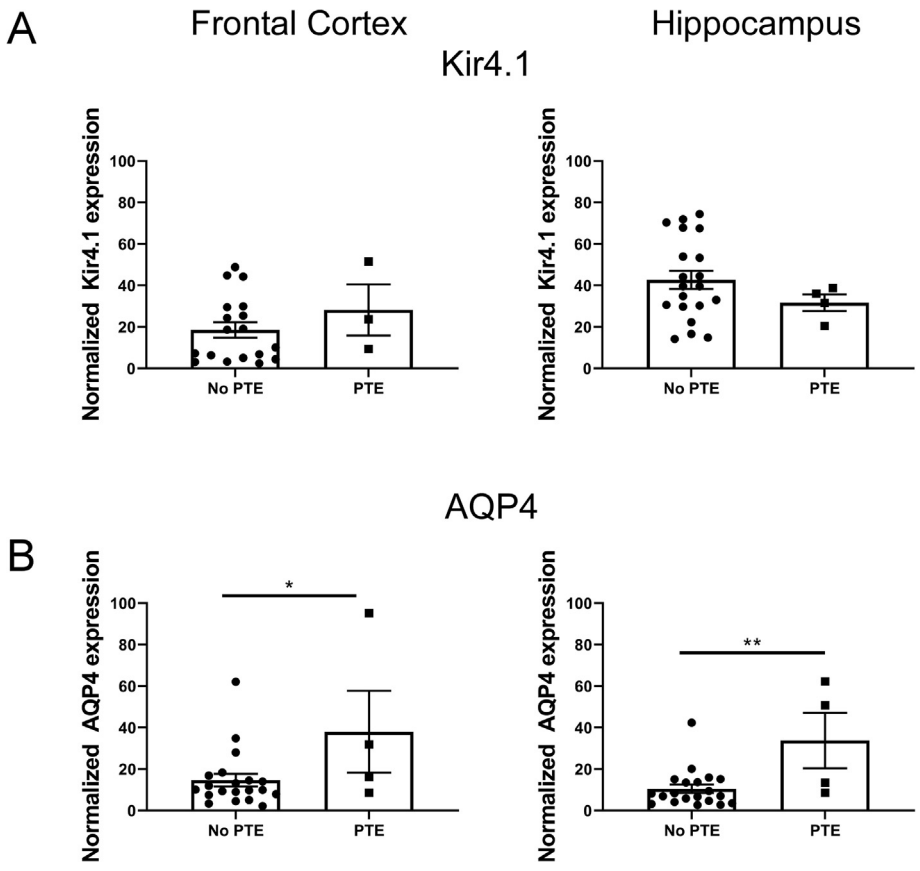

Fig. 6. AQP4 is upregulated in the frontal cortex and hippocampus of mice with PTE. (**A**) No significant differences in Kir4.1 protein levels were detected in the frontal cortex and hippocampus of mice with and without PTE. (**B**) A significant increase in AQP4 expression was detected in the frontal cortex (left) and hippocampus (right) of mice with PTE. Data was analyzed with Student's *t*-test. Error bars are mean ± SEM, $*p < 0.05$.

(or dysregulation) of AQP4 after TBI in both the injured cortex and hippocampus correlates with the development of PTE. Specifically, Kir4.1 does not seem to be a key player in PTE and rather neuronal hyperexcitability appears to be modulated by AQP4. This was an unanticipated finding as previous studies have suggested a direct functional interaction between AQP4 and Kir4.1 (Nagelhus et al., 2004; Connors and Kofuji 2006; Masaki et al., 2010); however others have disputed this hypothesis. For example, studies using AQP4 null mice or inhibition of Kir4.1 by barium or RNAi knock-down did not show any significant differences in membrane potential, barium-sensitive Kir4.1 potassium currents, or current–voltage curves using whole-cell patch clamp and single-channel patch clamp. No changes in Kir4.1 unitary conductances from glial cells isolated from WT and AQP4 null mice were detected as well (Ruiz-Ederra et al., 2007; Zhang and Verkman, 2008). Moreover, inhibition of Kir4.1 did not alter AQP4 dependent water permeability (Zhang and Verkman, 2008). Distinct AQP4 and Kir4.1 regulation was also previously reported in an intrahippocampal kainic acid (IHKA) model of TLE where induction of status epilepticus (SE) with kainic acid significantly downregulated AQP4 in the hippocampus whereas no significant alterations in Kir4.1 were observed (Lee et al., 2012).

Although AQP4 regulation has not been investigated in human and experimental models of PTE, increased levels of AQP4 have been previously reported in chronic studies of epilepsy. For example, altered expression and subcellular localization of AQP4 was found in postmortem sclerotic hippocampi from patients with mesial TLE (Eid et al., 2005). Although an overall increased AQP4 expression was found in the sclerotic hippocampus in human TLE (Lee et al., 2004), reduction in perivascular AQP4 was observed (Eid et al., 2005). However, we do not believe that the altered AQP4 expression we observed is due to gliosis as we did not detect any significant differences in GFAP immunoreactivity between sham and TBI mice at all time points (data not shown). Rather, we think that dysregulation of AQP4 is the primary risk factor we have identified in the development of posttraumatic epileptogenesis. Loss of perivascular AQP4 has also been previously reported in rodent models of TLE (Kim et al., 2009, 2010; Alvestad et al., 2013). In one study, levels of AQP4 in astrocytic endfeet facing capillaries were reduced 14 and 11 weeks after induction of status epilepticus (SE) (Alvestad et al., 2013). Furthermore, loss of perivascular AQP4 was also observed in a "hit and run" model of TBI in which reductions in perivascular AQP4 was observed as early as 3 dpi and up to 28 dpi (Ren et al., 2013). Loss or redistribution of AQP4 can lead to astrocyte endfeet swelling due to decreased efflux of water and K^+ from astrocyte endfeet into the blood vessels resulting in increased seizure susceptibility (Wetherington et al., 2008; Binder et al., 2012).

One mechanism underlying the loss of perivascular AQP4 may be due to impaired AQP4 surface trafficking. AQP4 exists as two principal isoforms: the long M1-AQP4 isoform and the short M23-AQP4 isoform (Neely et al., 1999). Early and recent findings have observed that these two isoforms exhibit different subcellular localization and distinct functions. For instance, M1-AQP4 diffuses freely on the plasma membrane and can localize to the leading edge of astrocytes to aid in migration (Smith et al., 2014). On the other hand, M23-AQP4 is generally immobile and is found to be highly expressed in astrocyte endfeet (Crane et al., 2008, Smith et al., 2014). Furthermore, it was recently found that hippocampal M23-AQP4 adapts to neuronal activity by upregulating

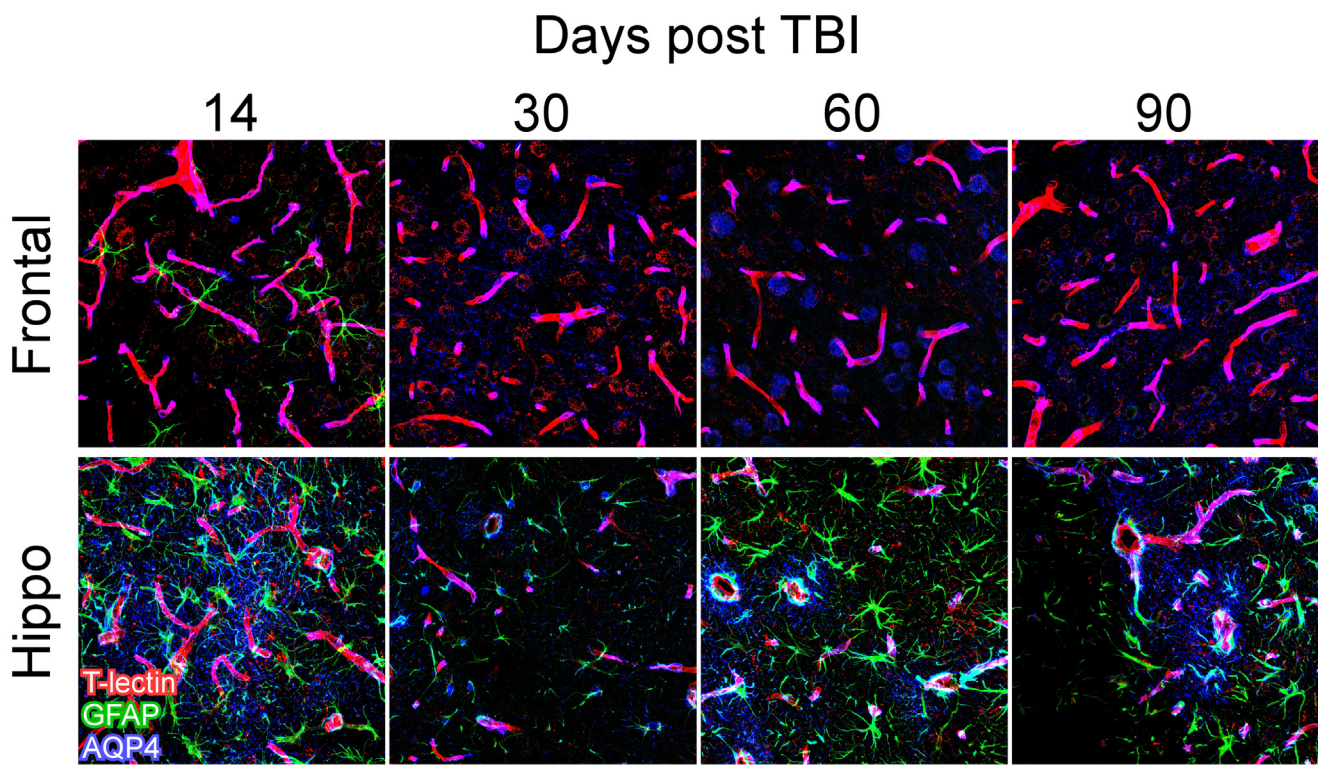

Fig. 7. Perivascular AQP4 is preserved in the frontal cortex and hippocampus of sham mice. AQP4 (blue) is colocalized with blood vessels (T-lectin, red) in the frontal cortex and hippocampus of sham mice at all time points. Perivascular AQP4 is represented as magenta color. AQP4 = aquaporin-4, GFAP = glial fibrillary acidic protein, T-lectin = tomato-lectin. Images taken at 63× and hippocampal images were obtained in the stratum radiatum and stratum lacunosum moleculare. (For interpretation of the references to color in this figure legend, the reader is referred to the web version of this article.)

astrocyte process motility and decreasing M23-AQP4 membrane trafficking. Indeed, this regulatory function was found to be impaired in patients with neuromyelitis optica (Ciappelloni et al., 2019). Therefore, the mislocalization of AQP4 that we observed may be due to deficits in M23-AQP4 trafficking. For instance, TBI may have caused an increase in M23-AQP4 membrane trafficking to diffuse away from the endfeet and towards the neuropil which leads to impaired water and ion homeostasis ultimately increasing neuronal hyperexcitability. We found that mislocalization of AQP4 was greatest at 14 dpi) with partial restoration of perivascular AQP4 at 30 dpi with full recovery at 60 dpi (Fig. 9). This suggests that AQP4 dysregulation, in particular M23-AQP4, at earlier time points may contribute to epileptogenesis at chronic time points. Indeed, by 90 dpi, the number of spontaneous seizures reduced from a total of 20 seizures at 60 dpi to six seizures at 90 dpi. In agreement with previous reports, loss of perivascular AQP4 may modulate seizure activity and contribute to overall epileptogenesis (Lee et al., 2012; Alvestad et al., 2013). In our studies, we found that perivascular AQP4 was mostly preserved in injured mice without PTE suggesting a possible functional protective role of AQP4 in which AQP4 was able to extrude water back into the vascular network maintaining overall water and ionic homeostasis. If this idea is validated in future studies, then restoration of AQP4 homeostasis after injury may represent an antiepileptogenic therapy after TBI.

Drawbacks and future studies

Although our findings demonstrating spontaneous hippocampal seizures after a single TBI in the frontal cortex are unique, we recognize there are drawbacks to our studies. First, the limited number of vEEG recording days can miss spontaneous seizures occurring at other times after TBI. While longitudinal long-term vEEG after TBI is most certainly useful and can provide beneficial information, analysis for such a large data set can be exhaustive and may require binning of the raw data, which may reduce the number of data analyzed. To overcome this challenge, we performed 1-week vEEG at various time points after injury to gain initial insight on hippocampal seizure pathology after TBI.

Another downside of our study is the use of only a single hippocampal electrode which can also lead to missed detection of spontaneous seizures occurring in other areas of the brain. Therefore, we have not yet determined whether posttraumatic seizures in our model are focal or global and if and when they can secondarily generalize. In the current study, we focused primarily on the hippocampus, a structure that is highly vulnerable to seizures. Studies have shown that PTE can manifest as TLE (Mathern et al., 1994; Diaz-Arrastia et al., 2000; Santhakumar et al., 2001) in which recurrent spontaneous seizures arises from the temporal lobe (Hubbard et al., 2013). Therefore,

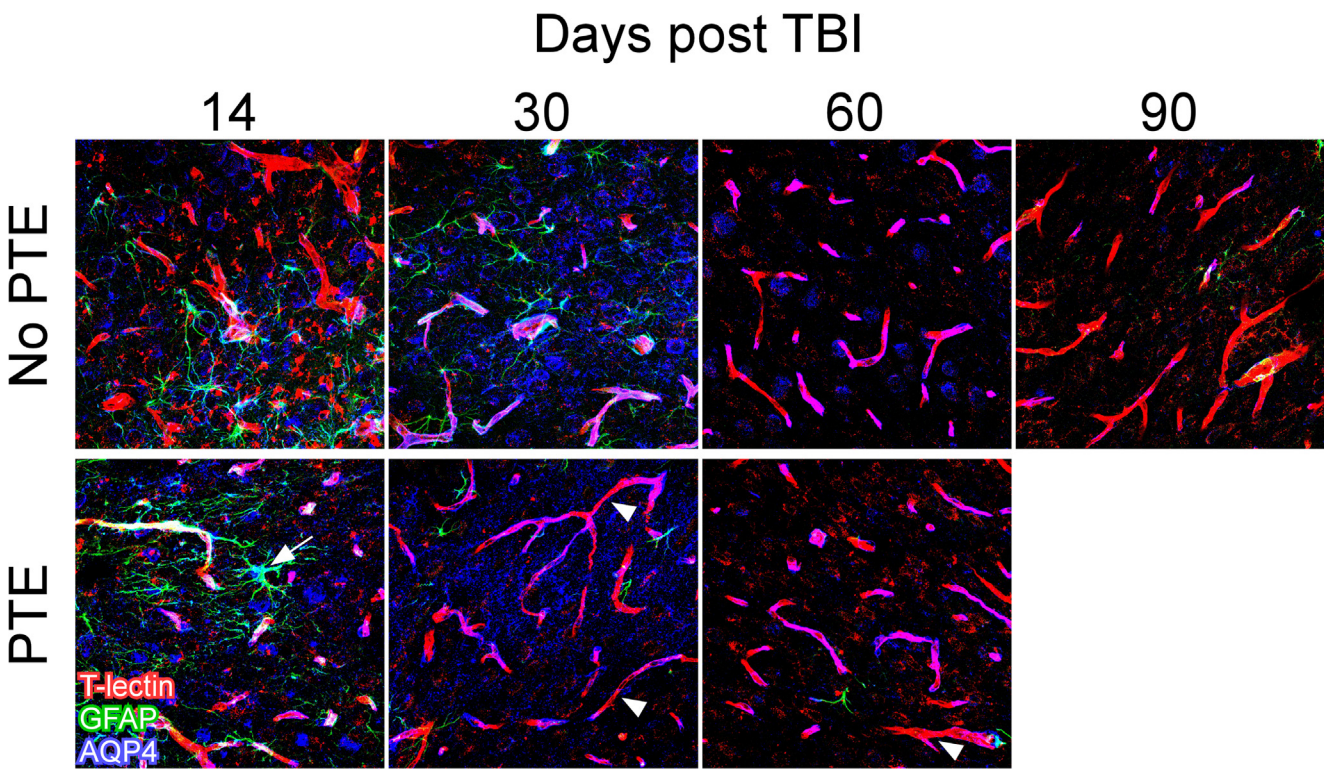

Fig. 8. Mislocalization of AQP4 in the frontal cortex of mice with PTE. In mice without PTE (top), AQP4 is partially redistributed. Specifically, loss of perivascular AQP4 is detected in the frontal cortex of mice without PTE at 14 and 90 dpi (red colored blood vessels showing lack of AQP4 colocalization), however, a partial recovery of perivascular AQP4 is observed at 30 and 60 dpi (magenta colored blood vessels indicating colocalization with perivascular AQP4). In mice with PTE (bottom) mislocalization of AQP4 is observed at 14 dpi (white arrow, cyan color showing colocalization of AQP4 (blue) with astrocyte (GFAP, green)), while AQP4 mislocalization is less prominent at 30 and 60 dpi with some vessels devoid of AQP4 (white arrow head on blood vessels (T-lectin)). AQP4 = aquaporin-4, GFAP = glial fibrillary acidic protein, T-lectin = tomato-lectin. Images taken at 63×. (For interpretation of the references to color in this figure legend, the reader is referred to the web version of this article.)

the development of TLE particularly after an injury in the frontal cortex is of great interest which has not been previously explored in detail.

Finally, while we classified mice with one seizure as not having PTE, we recognize that these mice may develop subsequent seizures or even have early seizures that we may not have captured. We understand that with limited vEEG recording days and the use of one electrode allows missed opportunity to define a more accurate incidence of PTE. However, our definition of PTE in this specific study has yielded unanticipated findings, in particular, significant differences in AQP4 expression levels in both the frontal cortex and hippocampus that may contribute to the development of posttraumatic epileptogenesis. Indeed, future studies with longer vEEG recordings and multiple electrodes such as the use of multi-electrode arrays (which covers the entire surface of the mouse skull) in conjunction with hippocampal depth electrodes can significantly improve characterization of PTE pathogenesis.

While PTE is of great clinical importance, the pathophysiology of PTE remains unknown. Preclinical studies must use translational models of PTE that reflect the human condition and detailed evaluation of electrophysiological and histological changes is urgently needed not only to determine the cellular and molecular changes underlying PTE, but to also define biomarkers for new therapeutic treatment development.

In the present study, we report, for the first time, the highest yield of PTE in mice after CCI using moderate-severe CCI at 1.0 mm impact depth in frontal cortex with chronic hippocampal vEEG recordings. Second, we are the first to report dysregulation of AQP4 in a model of PTE, specifically upregulation and mislocalization of perivascular AQP4 observed exclusively in mice that developed PTE. Collectively, these findings suggest that AQP4 is essential for modulating neuronal hyperexcitability following TBI and can serve as a foundation to create new astrocyte-based therapeutic strategies to prevent epileptogenesis after TBI.

FUNDING

This research did not receive any specific grant from funding agencies in the public, commercial, or not-for-profit sectors.

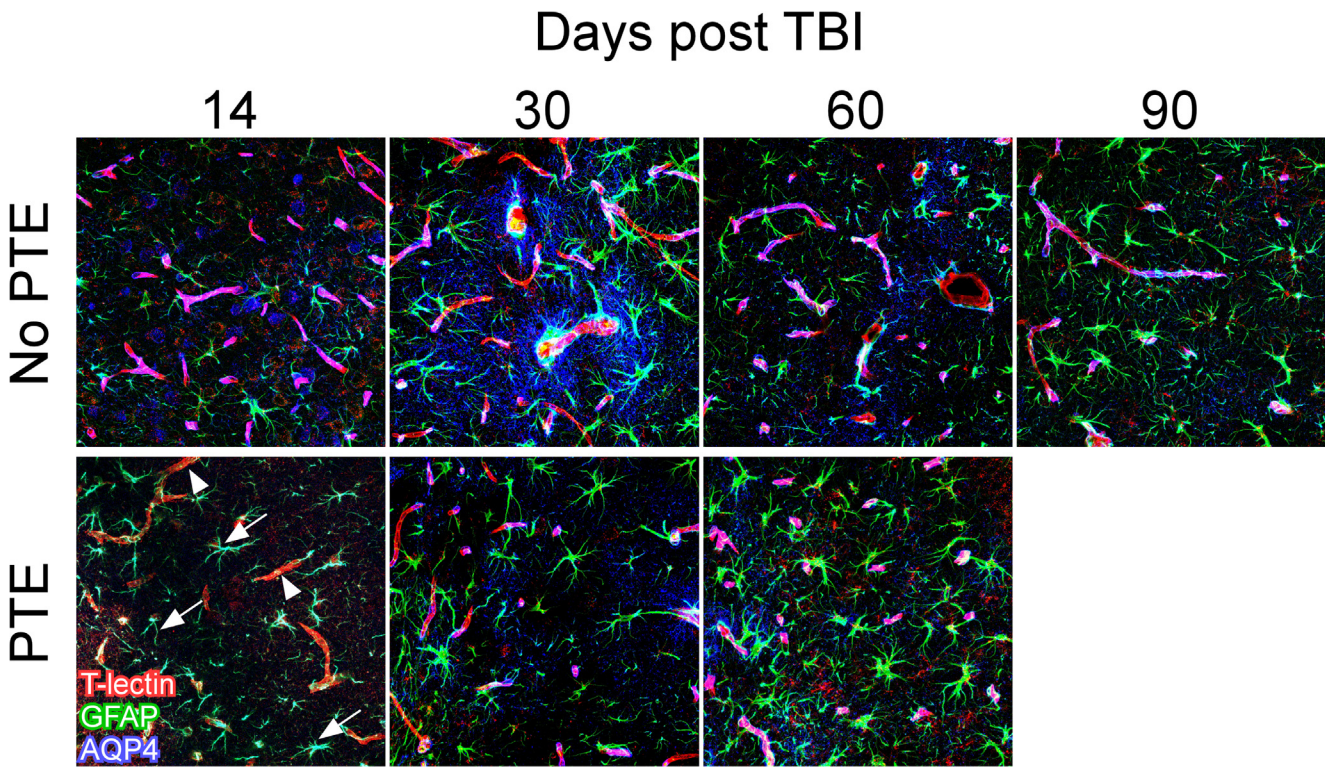

Fig. 9. Dysregulation of hippocampal AQP4 in mice with PTE. Perivascular AQP4 is maintained in the hippocampus of mice without PTE (top). AQP4 (blue) is primarily localized to blood vessels (T-lectin, red) in the hippocampus of mice without PTE at all time points suggesting a possible protective role of AQP4 in the development of PTE. In mice with PTE (bottom), AQP4 is found to be mislocalized at 14 dpi where AQP4 immunoreactivity is largely found in the soma and major processes of astrocytes (white arrow, cyan color showing colocalization of AQP4 with GFAP). Additionally, blood vessels (T-lectin, red) are completely lacking perivascular AQP4 at this time point (white arrowhead). At 30 dpi, partial recovery of perivascular AQP4 is observed (partial but not complete overlap of AQP4 and T-lectin immunoreactivity. At 60 dpi, perivascular AQP4 expression is observed by complete overlap of AQP4 and T-lectin immunoreactivity with no colocalization of AQP4 with astrocytes (GFAP, green). AQP4 = aquaporin-4, GFAP = glial fibrillary acidic protein, T-lectin = tomato-lectin. Images were taken at 63× and hippocampal images were taken from the stratum radiatum and stratum lacunosum moleculare. (For interpretation of the references to color in this figure legend, the reader is referred to the web version of this article.)

REFERENCES

Alvestad S, Hammer J, Hoddevik EH, Skare Ø, Sonnewald U, Amiry-Moghaddam M, Ottersen OP (2013) Mislocalization of AQP4 precedes chronic seizures in the kainate model of temporal lobe epilepsy. Epilepsy Res 105(1–2):30–41.

Annegers JF, Hauser WA, Coan SP, Rocca WA (1998) A population-based study of seizures after traumatic brain injuries. N Engl J Med 338(1):20–24.

Binder DK, Nagelhus EA, Ottersen OP (2012) Aquaporin-4 and epilepsy. Glia 60(8):1203–1214.

Bolkvadze T, Pitkänen A (2012) Development of post-traumatic epilepsy after controlled cortical impact and lateral fluid-percussion-induced brain injury in the mouse. J Neurotrauma 29 (5):789–812.

Cheung G, Sibille J, Zapata J, Rouach N (2015) Activity-dependent plasticity of astroglial potassium and glutamate clearance. Neural Plast 2015.

Chodobski A, Zink BJ, Szmydynger-Chodobska J (2011) Blood–brain barrier pathophysiology in traumatic brain injury. Transl Stroke Res 2(4):492–516.

Ciappelloni S, Bouchet D, Dubourdieu N, Boué-Grabot E, Kellermayer B, Manso C, Marignier R, Oliet SH, Tourdias T, Groc L (2019) Aquaporin-4 surface trafficking regulates astrocytic process motility and synaptic activity in health and autoimmune disease. Cell Rep 27(13):3860–3872. e3864.

Connors NC, Kofuji P (2006) Potassium channel Kir4. 1 macromolecular complex in retinal glial cells. Glia 53(2):124–131.

Crane JM, Van Hoek AN, Skach WR, Verkman A (2008) Aquaporin-4 dynamics in orthogonal arrays in live cells visualized by quantum dot single particle tracking. Mol Biol Cell 19(8):3369–3378.

Curia G, Levitt M, Fender JS, Miller JW, Ojemann J, D'Ambrosio R (2010) Impact of injury location and severity on posttraumatic epilepsy in the rat: role of frontal neocortex. Cereb Cortex 21 (7):1574–1592.

D'Ambrosio R, Fender JS, Fairbanks JP, Simon EA, Born DE, Doyle DL, Miller JW (2005) Progression from frontal–parietal to mesial–temporal epilepsy after fluid percussion injury in the rat. Brain 128 (1):174–188.

D'Ambrosio R, Fairbanks JP, Fender JS, Born DE, Doyle DL, Miller JW (2004) Post-traumatic epilepsy following fluid percussion injury in the rat. Brain 127(2):304–314.

D'Ambrosio R, Maris DO, Grady MS, Winn HR, Janigro D (1999) Impaired K+ homeostasis and altered electrophysiological properties of post-traumatic hippocampal glia. J Neurosci 19 (18):8152–8162.

Devinsky O, Vezzani A, Najjar S, De Lanerolle NC, Rogawski MA (2013) Glia and epilepsy: excitability and inflammation. Trends Neurosci 36(3):174–184.

Diaz-Arrastia R, Agostini MA, Frol AB, Mickey B, Fleckenstein J, Bigio E, Van Ness PC (2000) Neurophysiologic and neuroradiologic features of intractable epilepsy after traumatic brain injury in adults. Arch Neurol 57(11):1611–1616.

Dixon CE, Clifton GL, Lighthall JW, Yaghmai AA, Hayes RL (1991) A controlled cortical impact model of traumatic brain injury in the rat. J Neurosci Methods 39(3):253–262.
Donkin JJ, Vink R (2010) Mechanisms of cerebral edema in traumatic brain injury: therapeutic developments. Curr Opin Neurol 23 (3):293–299.
Eid T, Lee T-SW, Thomas MJ, Amiry-Moghaddam M, Bjørnsen LP, Spencer DD, Agre P, Ottersen OP, De Lanerolle NC (2005) Loss of perivascular aquaporin 4 may underlie deficient water and K+ homeostasis in the human epileptogenic hippocampus. Proc Natl Acad Sci U S A 102(4):1193–1198.
Engel Jr J (2001) A proposed diagnostic scheme for people with epileptic seizures and with epilepsy: report of the ILAE Task Force on Classification and Terminology. Epilepsia 42 (6):796–803.
Englander J, Bushnik T, Duong TT, Cifu DX, Zafonte R, Wright J, Hughes R, Bergman W (2003) Analyzing risk factors for late posttraumatic seizures: a prospective, multicenter investigation. Arch Phys Med Rehabil 84(3):365–373.
Golarai G, Greenwood AC, Feeney DM, Connor JA (2001) Physiological and structural evidence for hippocampal involvement in persistent seizure susceptibility after traumatic brain injury. J Neurosci 21(21):8523–8537.
Guo D, Zeng L, Brody DL, Wong M (2013) Rapamycin attenuates the development of posttraumatic epilepsy in a mouse model of traumatic brain injury. PLoS ONE 8(5) e64078.
Guo Q, Sayeed I, Baronne LM, Hoffman SW, Guennoun R, Stein DG (2006) Progesterone administration modulates AQP4 expression and edema after traumatic brain injury in male rats. Exp Neurol 198(2):469–478.
Hauser WA, Annegers JF, Kurland LT (1993) Incidence of epilepsy and unprovoked seizures in Rochester, Minnesota: 1935–1984. Epilepsia 34(3):453–468.
Heuser K, Eid T, Lauritzen F, Thoren AE, Vindedal GF, Taubøll E, Gjerstad L, Spencer DD, Ottersen OP, Nagelhus EA (2012) Loss of perivascular Kir4. 1 potassium channels in the sclerotic hippocampus of patients with mesial temporal lobe epilepsy. J Neuropathol Exp Neurol 71(9):814–825.
Hubbard JA, Hsu MS, Fiacco TA, Binder DK (2013) Glial cell changes in epilepsy: overview of the clinical problem and therapeutic opportunities. Neurochem Int 63(7):638–651.
Hudak AM, Trivedi K, Harper CR, Booker K, Caesar RR, Agostini M, Van Ness PC, Diaz-Arrastia R (2004) Evaluation of seizure-like episodes in survivors of moderate and severe traumatic brain injury. J Head Trauma Rehabil 19(4):290–295.
Hunt RF, Scheff SW, Smith BN (2009) Posttraumatic epilepsy after controlled cortical impact injury in mice. Exp Neurol 215 (2):243–252.
Hunt RF, Scheff SW, Smith BN (2010) Regionally localized recurrent excitation in the dentate gyrus of a cortical contusion model of posttraumatic epilepsy. J Neurophysiol 103(3):1490–1500.
Ihara Y, Tomonoh Y, Deshimaru M, Zhang B, Uchida T, Ishii A, Hirose S (2016) Retigabine, a Kv7. 2/Kv7. 3-channel opener, attenuates drug-induced seizures in knock-in mice harboring Kcnq2 mutations. PLoS ONE 11(2) e0150095.
Jennett WB, Lewin W (1960) Traumatic epilepsy after closed head injuries. J Neurol Neurosurg Psychiatry 23(4):295.
Kharatishvili I, Nissinen J, McIntosh T, Pitkänen A (2006) A model of posttraumatic epilepsy induced by lateral fluid-percussion brain injury in rats. Neuroscience 140(2):685–697.
Kim J-E, Ryu H, Yeo S-I, Seo C, Lee B, Choi I-G, Kim D-S, Kang T-C (2009) Differential expressions of aquaporin subtypes in astroglia in the hippocampus of chronic epileptic rats. Neuroscience 163 (3):781–789.
Kim JE, Yeo SI, Ryu HJ, Kim MJ, Kim DS, Jo SM, Kang TC (2010) Astroglial loss and edema formation in the rat piriform cortex and hippocampus following pilocarpine-induced status epilepticus. J Comp Neurol 518(22):4612–4628.
Kofuji P, Newman E (2004) Potassium buffering in the central nervous system. Neuroscience 129(4):1043–1054.
Lapato AS, Szu JI, Hasselmann JPC, Khalaj AJ, Binder DK, Tiwari-Woodruff SK (2017) Chronic demyelination-induced seizures. Neuroscience 346:409–422.
Lee DJ, Hsu MS, Seldin MM, Arellano JL, Binder DK (2012) Decreased expression of the glial water channel aquaporin-4 in the intrahippocampal kainic acid model of epileptogenesis. Exp Neurol 235(1):246–255.
Lee TS, Eid T, Mane S, Kim JH, Spencer DD, Ottersen OP, De Lanerolle NC (2004) Aquaporin-4 is increased in the sclerotic hippocampus in human temporal lobe epilepsy. Acta Neuropathol 108(6):493–502.
Lowenstein DH (2009) Epilepsy after head injury: an overview. Epilepsia 50(Suppl 2):4–9.
Maas AI, Stocchetti N, Bullock R (2008) Moderate and severe traumatic brain injury in adults. Lancet Neurol 7(8):728–741.
MacAulay N, Zeuthen T (2012) Glial K+ clearance and cell swelling: key roles for cotransporters and pumps. Neurochem Res 37 (11):2299–2309.
Manley GT, Binder D, Papadopoulos M, Verkman A (2004) New insights into water transport and edema in the central nervous system from phenotype analysis of aquaporin-4 null mice. Neuroscience 129(4):981–989.
Masaki H, Wakayama Y, Hara H, Jimi T, Unaki A, Iijima S, Oniki H, Nakano K, Kishimoto K, Hirayama Y (2010) Immunocytochemical studies of aquaporin 4, Kir4. 1, and α1-syntrophin in the astrocyte endfeet of mouse brain capillaries. Acta Histochemi Cytochem 43 (4):99–105.
Mathern GW, Babb TL, Vickrey BG, Melendez M, Pretorias JK (1994) Traumatic compared to non-traumatic clinical-pathologic associations in temporal lobe epilepsy. Epilepsy Res 19 (2):129–139.
Nagelhus E, Mathiisen T, Ottersen O (2004) Aquaporin-4 in the central nervous system: cellular and subcellular distribution and coexpression with KIR4. 1. Neuroscience 129(4):905–913.
Nagelhus EA, Horio Y, Inanobe A, Fujita A, Haug FM, Nielsen S, Kurachi Y, Ottersen OP (1999) Immunogold evidence suggests that coupling of K+ siphoning and water transport in rat retinal Müller cells is mediated by a coenrichment of Kir4. 1 and AQP4 in specific membrane domains. Glia 26(1):47–54.
Nagelhus EA, Ottersen OP (2013) Physiological roles of aquaporin-4 in brain. Physiol Rev 93(4):1543–1562.
Neely JD, Christensen BM, Nielsen S, Agre P (1999) Heterotetrameric composition of aquaporin-4 water channels. Biochemistry 38(34):11156–11163.
Nilsson P, Ronne-Engström E, Flink R, Ungerstedt U, Carlson H, Hillered L (1994) Epileptic seizure activity in the acute phase following cortical impact trauma in rat. Brain Res 637(1–2):227–232.
Orkand RK (1986) Introductory remarks: glial-interstitial fluid exchange. Ann N Y Acad Sci 481(1):269–272.
Pitkänen A, McIntosh TK (2006) Animal models of post-traumatic epilepsy. J Neurotrauma 23(2):241–261.
Pohlmann-Eden B, Bruckmeir J (1997) Predictors and dynamics of posttraumatic epilepsy. Acta Neurol Scand 95(5):257–262.
Raymont V, Salazar AM, Lipsky R, Goldman D, Tasick G, Grafman J (2010) Correlates of posttraumatic epilepsy 35 years following combat brain injury. Neurology 75(3):224–229.
Ren Z, Iliff JJ, Yang L, Yang J, Chen X, Chen MJ, Giese RN, Wang B, Shi X, Nedergaard M (2013) 'Hit & Run' model of closed-skull traumatic brain injury (TBI) reveals complex patterns of post-traumatic AQP4 dysregulation. J Cereb Blood Flow Metab 33 (6):834–845.
Ruiz-Ederra J, Zhang H, Verkman A (2007) Evidence against functional interaction between aquaporin-4 water channels and Kir4. 1 potassium channels in retinal Müller cells. J Biol Chem 282 (30):21866–21872.
Salazar AM, Jabbari B, Vance SC, Grafman J, Amin D, Dillon J (1985) Epilepsy after penetrating head injury. I. Clinical correlates A report of the Vietnam Head Injury Study. Neurology 35 (10):1406.

Santhakumar V, Ratzliff AD, Jeng J, Toth Z, Soltesz I (2001) Long-term hyperexcitability in the hippocampus after experimental head trauma. Ann Neurol 50(6):708–717.

Shandra O, Winemiller AR, Heithoff BP, Munoz-Ballester C, George K, Benko MJ, Zuidhoek I, Besser MN, Curley DE, Edwards GF (2019) Repetitive diffuse mild traumatic brain injury causes an atypical astrocyte response and spontaneous recurrent seizures. J Neurosci:1018–1067.

Smith AJ, Jin B-J, Ratelade J, Verkman AS (2014) Aggregation state determines the localization and function of M1–and M23–aquaporin-4 in astrocytes. J Cell Biol 204(4):559–573.

Steinhäuser C, Seifert G, Bedner P (2012) Astrocyte dysfunction in temporal lobe epilepsy: K+ channels and gap junction coupling. Glia 60(8):1192–1202.

Tait MJ, Saadoun S, Bell BA, Papadopoulos MC (2008) Water movements in the brain: role of aquaporins. Trends Neurosci 31 (1):37–43.

Temkin NR (2003) Risk factors for posttraumatic seizures in adults. Epilepsia 44:18–20.

Verkman A, Binder DK, Bloch O, Auguste K, Papadopoulos MC (2006) Three distinct roles of aquaporin-4 in brain function revealed by knockout mice. Biochim Biophys Acta (BBA)-Biomembranes 1758(8):1085–1093.

Werner C, Engelhard K (2007) Pathophysiology of traumatic brain injury. BJA: Br J Anaesth 99(1):4–9.

Wetherington J, Serrano G, Dingledine R (2008) Astrocytes in the epileptic brain. Neuron 58(2):168–178.

Zhang H, Verkman A (2008) Aquaporin-4 independent Kir4. 1 K+ channel function in brain glial cells. Mol Cell Neurosci 37(1):1–10.

(Received 22 October 2019, Accepted 3 December 2019)
(Available online 19 December 2019)